

Hazardous Bauxite Red Mud and Ferrous Slag Management to Produce Sustainable Construction Materials

*Vsevolod Mymrin**, Kirill Alekseev, Walderson Klitzke, Daniela E. Evaniki, Cleber L Pedroso, Fernando H Passig, Karina Q Carvalho, Charles W I Haminiuk, Rodrigo E Catai

Federal University of Technology - Parana (UTFPR), deputy Hector Alencar Furtado str., 4900, Curitiba, Paraná, Brazil

*Corresponding author

Vsevolod Mymrin

Federal University of Technology - Parana (UTFPR), deputy Hector Alencar Furtado str, 4900, Curitiba, Paraná, Brazil; Tel: 55-41-3279-6818

Email: seva6219@gmail.com

Received : January 10, 2023

Published : March 06, 2023

ABSTRACT

This paper reports the development and characterization of new ceramics from hazardous bauxite red mud (50 to 100 wt. %) and blast furnace slag (10 and 50%). The research aimed to demonstrate the possibility of expanding the base of powder raw materials for production of ceramics, completely replacing the traditional clay and sand with composites made from hazardous industrial wastes, which provide increasing local and global sustainability. The investigation of the physical-chemical changes in the ceramics structure was conducted by the AAS, XRD, SEM, XRF, LAMMA, and EDS tests. Changes in water absorption, density, linear shrinkage, and flexural strength were determined while the sintering processes ranged from 1,000° to 1,225 °C. Flexural strength reached 19.78 MPa after sintering at 1,225°C due to the syntheses of new structure formations, mainly similar to glass, confirmed by the characterization methods used, attesting to the complete binding of heavy metals.

Keywords: Hazardous bauxite red mud; ferrous slags; industrial waste recycling; environment protection; construction materials

INTRODUCTION

In one of his interviews, the most celebrated modern-day cosmologist, [1] said that “pollution and human “stupidity” remained the greatest threats to humankind.” He claimed that air pollution had increased 8% within the last five years, and the authors of this paper are convinced that most of that is due to municipal and industrial wastes.

According to the authors of this article, the best strategic way to prevent or postpone as much as possible this global ecological tragedy, scientifically predicted by Hawking, is to replace the raw materials with industrial waste. Hawking calculated that, at the current pace, the temperature of the atmosphere would rise, leading to the death of humankind in the next 300 years. It is known that the most significant air pollutants come from

industrial and municipal waste dumps. From this, it follows that scientifically based waste disposal will be a crucial factor for the survival of humanity.

The residues from bauxite processing, called red mud (RM), are generated during the obtaining of aluminum oxide from the bauxite ore by the Bayer process. The World Aluminum database [2] mentions that approximately 15 to 20 million tons of aluminum wastes (RM) have been discharged into industrial wastes worldwide. In Hungary, an RM storage dam collapsed, flooding the streets with red mud, killing ten people [3]. There are two main reasons to classify this red mud as a hazardous material: the first one is the high pH of sodium oxide followed by the heavy metals content (Cd, Pb, Cu, Cr, Zn).

Other similar accidents have occurred involving these types of waste. The two most recent of them, in 2015 and 2019, were the overflow of iron ore tailings in Brazil [4]. The number of their victims is hundreds of people, and the economic damage is in the order of several billion dollars.

The storage of wastes presents the risk of further accidents, forcing us to accept the need to recycle or reuse them instead of storing them. This paper presents a practical, scientifically based solution to the problem of hazardous RM by using it in different composites with ferrous slag (FS) to produce environmentally clean ceramics.

Some articles have been written [5,6] describing the physical-chemical characteristics of RM to find its best use. It is possible to use RM to remove Mn and As from drinking water; or as an adsorbent for enhancing ferricyanide removal [7]; or in mixes with fly ash to reduce CO₂ emissions [8,9] suggested mixtures of natural clay and RM, and investigated their optimal proportions [10]. Treated RM for the extraction of metals and other elements. The main flaw in this approach was that it led to the generation of more massive amounts of residue. It is possible to use RM in cementitious materials production [11] and as component of geopolymer composites [12]. Based on the characterization of Azevedo, et al [13] came to conclusion that it has potential for use in alternative construction materials.

Globally, the manufacture of 1.65 billion tonnes of iron and steel gives rise to the co-production of more than 567 million tonnes of metallurgical slag [14]. Blast furnace slag (FS) from steel production already has some forms of implementation as a raw material. [15] used it for binding materials' production; [16] formulated compositions with high contents of heavy

metals with ornamental rocks solid waste. Solidification and stabilization of galvanic solid waste, concomitantly with ornamental rocks solid waste. There are many published studies on methods [17] and effectiveness [18] of heavy metals adsorption from diverse industrial wastes. [19,20] used copper slag and municipal solid waste fly ashes and to produce traditional ceramic tiles with the immobilization of As and Pb. [21] found that it was suitable as a cementitious material for natural soils for road base construction to replace the two traditional base layers - sand and rubble - with a substantial increase in road resistance. Furnace slag (FS) was added to ceramic mixtures [22, 23]. The above review of the scientific and technical literature shows the originality of our ceramic compositions, which consist of only two types of hazardous industrial waste for the production of sustainable ceramic materials.

Three main objectives were sought in this study: 1. To develop new composites using only red mud (RM) and ground cooled blast furnace slag (FS), replacing the traditional known raw materials such as sand and natural clay (CSM); 2. To develop ceramics that meet Brazilian standards for physical, mechanical, and environmental properties; 3. To study and to intensify the processes involved in the new structures formation, responsible for the achievement of these properties in ceramics.

Therefore, the novelty of this study lies in the development of sustainable ceramic materials from two hazardous industrial wastes (bauxite red mud and ground cooled ferrous slag) with high values of physical, mechanical and environmental properties without the application of traditional natural components; the structure formation process of these materials, explaining the reasons of these properties appearance, was studied.

METHODS AND MATERIALS

Methods

XRF method was conducted to find the chemical composition of the materials, XRD determined the mineralogical composition, and the morphological structure was observed by SEM analysis. In order to identify the microchemical composition of individual particles of the material, EDS analyses were performed. LAMMA method determined the isotropic composition. AAS was used to investigate possible solubilized and leached metals; the particle size distribution was determined by laser analysis. Completing the studies,

flexural resistance, linear shrinkage, water absorption, and density were also performed.

The manufacture of ceramics was under the following steps: mixing the components according to the pre-established composition (Table 1); addition of water (12-14%) to plasticize the mixes; compression of wet samples at 5 MPa, in rectangular press-forms of 60 x 20 x 10mm size, drying to constant weight at 100°C, sintering for 3 hours (temperatures of 800°, 900°, 1000°, 1050°, 1100°, 1150°, 1200°, and 1225°C), and cooling by natural convection.

The chemical composition was studied by the X-ray fluorescence (XRF) method, using a Philips/ Panalytical PW 2400 model, and by atomic absorption spectroscopy (AAS), using the Perkin Elmer 4,100 spectrometer. The granulometric composition was measured by laser diffraction particle size distribution analysis with an LA-950 HORIBA Analyzer and by the sieve method; the mineral composition was measured by X-ray diffraction (XRD) with the Philips PW 1830 model. The morphological structure was analyzed by scanning electron microscopy (SEM) with a Quanta FEI 200 LV microscope. The chemical micro analyses were carried out by energy dispersive spectroscopy (EDS) (Penta FET-Precision) and by micro-mass analyses using an X-ACT LAMMA-1000 laser micro-mass analyzer. The solubility and metals lixiviation from liquid

extracts were determined by atomic spectroscopy analyses (ASA) with a Perkin Elmer 4100 spectrometer (Mitutoyo). Mechanical uniaxial resistance strength was verified by a universal testing machine (EMIC DL10,000); the water absorption measured by Instrutherm BD 200 equipment, and the linear expansion was ascertained by a digital caliper.

The average values of all properties were calculated from five determinations with the calculation of deviations from the average.

RESEARCH RESULTS AND DISCUSSION

Characterization

The characterization was conducted in order to determine the granulometric, mineral and chemical compositions, and morphological microstructure of the studied materials.

Chemical composition and particles size distribution

Both industrial wastes used as raw materials in the study were obtained from local factories in Brazil. The natural clay sample, mixed with 10% of sand, was obtained at a local ceramics production plant and was used in this work only as a generally accepted industry standard.

Table 1: Chemical composition of the raw materials.

Oxides	Components (wt. %)			Oxides	Components (wt. %)		
	RM	FS	NC		RM	FS	NC
Fe ₂ O ₃	29.9	62.1	6.1	Cr ₂ O ₃	< 0.1	0.3	< 0.1
SiO ₂	15.5	13.8	53.3	V ₂ O ₅	0.1	0.0	< 0.1
SO ₃	0.6	10.0	0.1	BaO	0.0	0.2	0.1
Al ₂ O ₃	21.2	2.6	24.7	P ₂ O ₅	0.0	0.1	0.0
CaO	4.2	2.5	0.4	SnO ₂	0.0	0.1	0.0
MgO	0.1	0.3	0.7	ZnO	< 0.1	0.1	< 0.1
Na ₂ O	10.3	0.9	0.1	CuO	0.0	0.1	0.0
K ₂ O	0.4	0.4	1.0	ZrO ₂	0.2	< 0.1	0.1
MnO	0.2	0.6	0.1	MoO ₃	0.0	< 0.1	0.0
TiO ₂	2.4	0.4	1.4	I.L.	14.4	1.7	11.5
P ₂ O ₅	0.6	3.5	0.1	Total	100.0	100.0	100.0

XRF method showed that RM consisted mainly of Fe₂O₃ (29.9 %), followed by Al₂O₃ (21.2%), SiO₂ (15.5%), and Na₂O (10.3%) (Table 1). The high ignition loss value (14.36%) of the

RM might be explained by the carbonates content, by some hydroxide OH-group and water content after undergoing Bayer's thermochemical process for bauxite ore treatment.

The metals Ni (1.26%), Sn (1.18%), Ba (0.79%), Zn (0.72%), found by the AAS method, exceeded the relevant Brazilian standards [24]. RM is classified as a hazardous waste due to its high pH value (13.5) and the presence of high heavy metals content. FS

contained extremely high amounts of ferrous oxides (62.1%) in addition to SiO₂ (13.8%) and SO₃ (10.0%), Al₂O₃ (2.6%), and CaO (2.5%).

Table 2: Grain size distribution in weight %, tapped density in g/cm³, and humidity (%) of the raw materials under study.

Grain size distribution	Size (mm)	Red mud	Furnace slag	Natural clay
	0 - 0.074	0.32	1.35	89.76
	0.075 - 0.149	1.08	17.63	5.68
	0.15 - 0.29	13.14	66.39	3.17
	0.3 - 0.59	46.13	14.63	1.39
	0.6 - 1.19	39.33	0.00	0
	≥1.2	0.00	0.00	0
Tapped density (g/cm³)		0.86	2.75	1.56
Humidity		32.2	3.1	9.34
Compositions, wt.%		Flexural strength (MPa) of ceramics after sintering at T°C		

The grain size classification (Table 2) showed that RM had a total of particles between 0.3 and 1.2 mm equal to 85.46%. The majority of FS particles (85.37%), on the contrary, presented sizes between 0 and 0.29mm.

Mineralogical composition

The mineralogical compositions of the raw materials, analyzed by the XRD method (Figure1), were also somewhat different: RM held magnetite Fe₃O₄, hematite Fe₂O₃, bauxite Al₂O₃·nH₂O, and quartz SiO₂, while FS held fayalite Fe₂·2SiO₄ and troilite FeS.

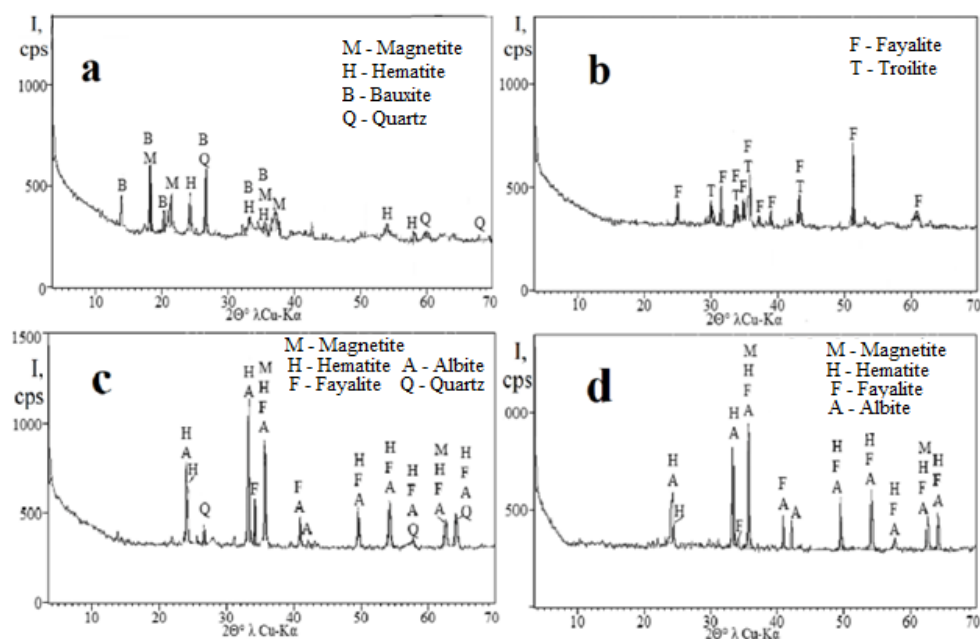


Figure 1: XRD patterns of the raw materials: **a** – red mud, **b** – blast furnace slag, and of the ceramics 7 after sintering at: **c**- 1000°C and **d** - at 1225°C.

Both raw materials showed very weak crystal peaks and very robust X-Ray backgrounds due to the meager of crystalline structures and predominance of amorphous structures.

Thermic characteristics of the raw materials under study

The endothermic effect between 194°C and 279°C (Figure2) correlated with the endothermic effect of the red mud between 202°C and 296°C, which denoted a decrease in the loss of crystal structure water of gibbsite $Al(OH)_3$ with its transition to boehmite $\gamma-AlO(OH)_4$. The weight loss during this reaction of composition 7 was significantly lower (2.13%) than that of red mud (5.36%). The reason for this might be the content of 50% red mud in the original mixture and the imprecision of

the selected points of the initial and final temperatures in the DTA and TGA curves.

The second endothermic effect of composition 7, between 279°C and 392°C with low tolerance, replicated another endothermic effect of the red mud between 296°C and 431°C. The concurrence of their weight loss values 1.50% and 3.10% was also quite logical and corresponded to the conversion reaction of boehmite $\gamma-AlO(OH)_4$ in anhydrous $\gamma-Al_2O_3$ [25,26]. The sharp peak of the exothermic reaction between 469°C and 582°C with a weight loss corresponded to 2.23% two-headed blast furnace slag exothermic effect at 413° - 560°C with atotal weight loss of 1.47%.

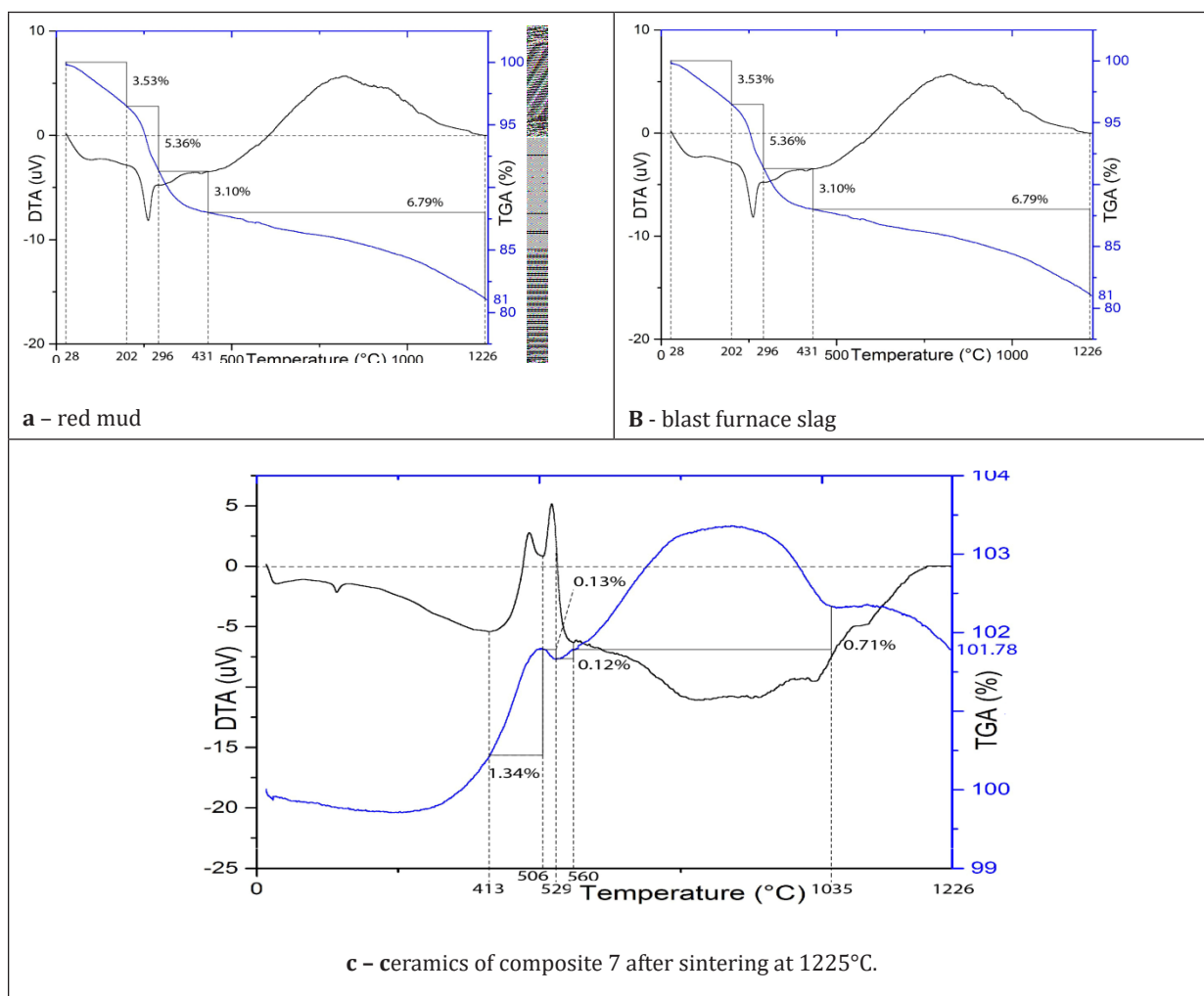


Figure 2: DTA and TGA curves of red mud, blast furnace slag

The presence of 10.0% SO₃ and high iron content (62.1%) in the chemical composition of the blast furnace slag inevitably led to their combination during composition 7's heating in the forms of iron hydrates, iron sulfates, and iron sulfides.

A mild exothermic effect on red mud's DTA curve between 582°C and 735°C along with a 1.61% weight gain on TGA curve was probably due to the transition of anhydrous boehmite $\gamma\text{-Al}_2\text{O}_3$ to $\alpha\text{-Al}_2\text{O}_3$. There was also a chain of transitions in the blast furnace slag $\text{FeOOH} \rightarrow \gamma\text{-Fe}_2\text{O}_3 \rightarrow \text{Fe}_3\text{O}_4$ at the same temperature [27], related to the $\text{Fe}_2(\text{SO}_4)_3$ melting and to the beginning of the combustion the SO₂ gas, which was formed due to the transition of $\text{Fe}_2(\text{SO}_4)_3$ to Fe_2O_3 . The appearance of this exothermic effect in the blast furnace slag corresponded to thermochemical decomposition of FeS₂ by oxidation with the following transfer to $\text{FeSO}_4 + \text{SO}_2$ and burning of the released gas. Typically, this reaction takes place at 630-650°C, which coincided with the peak's turning point at an environment of 582°-735°C. The total weight increase was equal to 2.33%. The

third exothermic effect of composition 7 occurred at 735° - 1227°C and involved four different thermochemical reactions: The transition $\gamma\text{-Al}_2\text{O}_3 \rightarrow \alpha\text{-Al}_2\text{O}_3$; the transition $\text{Fe}_3\text{O}_4 \rightarrow \text{Fe}$ up to 700-750 °C; reduction in sample weight as a result of the final SO₂ release and burning of the released gas; the formation of Fe₃O₄. The total weight loss of these processes was 4.43%.

Probably, the formation of iron dross and the SO₂ combustion process imparted the darkening of the samples, which appeared at temperatures of 1200°C - 1225°C. The maximum intensity of these processes at 1225°C resulted in maximum flexural strength.

Morphological structures

The morphological structures of the particles suggest a wide variety of shapes, sizes, and forms of the grains of all materials, which meant that there was no uniform structure (Figure3). Such particle morphology indicated a predominantly amorphous

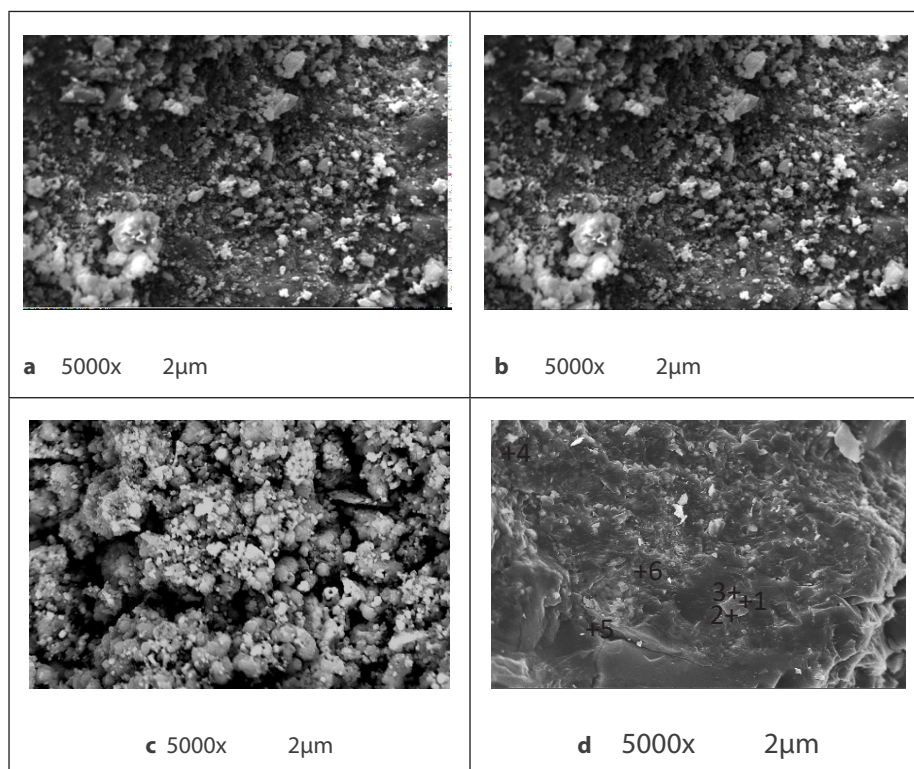


Figure 3: Micro-structures of the RM (A), FS (B) and composite 7 after sintering at 1000° (C) and 1225°C (D) with EDS analyses points.

Structure of the materials, established by the XRD method. All of them were disconnected and had no chemical bonds between them. A significant difference was observed between RM and FS regarding compositions (chemical and mineralogical) and particle structure.

Physical properties of new ceramics

The ceramics flexural strength changes, linear shrinkage, water absorption, and apparent density were looked into after sintering at different temperatures to characterize their

physical properties.

Flexural strength of new ceramics

Red mud was the principal component of this study. It contained the remains of the alkaline reagent from bauxite ore decomposition (hydroxide NaOH) (Table 1), having a melting point (T_m) of 323°C. This occurrence led to the formation of chemical compounds, such as NaHCO_3 ($T_m = 270^\circ\text{C}$), Na_2CO_3 ($T_m = 852^\circ\text{C}$) and Na_2SO_4 ,

Table 3: Flexural resistance strength after sintering at different temperatures (°C).

№	Compositions, wt.%			Flexural strength (MPa) of ceramics after sintering at T°C							
	NC	RM	FS	800	900	1000	1050	1100	1150	1200	1225
1	100	0	0	5.36	5.68	7.09	8.72	10.08	14.65	13.36	6.05
2	0	100	0	0	0	0.45	0.93	4.34	6.06	12.17	12.32
3	0	90	10	2.21	2.66	3.13	4.24	5.51	7.42	12.27	13.10
4	0	80	20	2.27	2.44	2.64	3.62	4.65	7.81	14.28	15.96
5	0	70	30	1.26	2.08	2.34	3.15	4.72	8.49	10.65	16.36
6	0	60	40	1.21	1.67	2.26	4.30	5.01	8.10	10.11	18.05
7	0	50	50	1.59	2.17	3.34	5.39	8.12	13.05	15.55	19.78

($T_m=883^\circ\text{C}$). Therefore, these chemical species might serve as flux components during the ceramics firing process, reducing it. Comparing the tiny increase in RM flexural strength values (Table 3) at 1200°C (12.17 MPa) and 1225°C (12.32 MPa), it may be stated that, at about 1225°C, the RM was very close to exceeding its melting point. An increase in FS content drove to a decrease in the flux of RM content and an increment in the temperature, favoring the excessive melting of ceramics.

Therefore, ceramics 7, with the highest slag content (50%), had the highest strength (19.78 MPa) after 1225°C firing; and ceramics 2 (without slag) and 3 (with 10% slag content) showed the lowest resistance (12.32 MPa and 13.10 MPa, respectively).

Solid bricks are classified by [28] according to their flexural strength in three classes: Class A < 2.5 MPa; Class B from 2.5 to 4.0 MPa; and Class C > 4.0 MPa. It means that practically

all developed ceramics met the demands of Class A (< 2.5 MPa) after 800°C sintering. Ceramics 3 met the requirements of Class B (2.5 - 4.0 MPa) after 900°C as well as ceramics 4 and 7 after 1000°C and ceramics 5 after 1050°C. Ceramics 3, 6, and 7 after 1050°C corresponded to the demands of Class C, as well as all other ceramics after sintering at 1100° C. All ceramics significantly exceeded the demands of class C (> 4.0 MPa) after firing at 1150°C. The values of standard deviations of flexural resistance strength of samples varied between 0.5 and 1.2 MPa.

Water absorption and apparent density

The water absorption value is an indirect indicator of the open porosity of materials, so the changes in water absorption (Table 4) were also strongly linked to changes in flexural strength. The water absorption values decreased with the temperature rise due to a more intense process of closure of the open pores.

Table 4: The water absorption value of the developed ceramics.

№	Composites, wt.%			Water absorption (%) of ceramics at different temperatures (°C)							
	CSM	RM	BFS	800	900	1,000	1,050	1,100	1,150	1,200	1,225
1	100	0	0	20.40	20.00	18.49	15.26	12.76	10.53	8.78	8.10
2	0	100	0	33.78	31.36	28.68	25.79	24.62	19.98	11.79	9.31
3	0	90	10	27.65	27.28	27.86	22.86	20.51	17.03	9.67	6.14
4	0	80	20	28.65	26.35	24.90	21.67	19.49	16.12	8.41	4.56
5	0	70	30	22.66	24.94	23.19	22.48	18.92	14.23	7.29	2.29
6	0	60	40	26.94	25.14	20.29	19.22	17.17	11.04	5.64	1.45
7	0	50	50	23.37	19.63	17.09	16.73	14.68	9.16	2.86	2.09

Composition 7, with the maximum amount of slag, showed the lowest water absorption values at all sintering temperatures; the maximum value was found in composition 2 (100% RM). The values decreased from 33.78 to 2.09%, with standard deviations values between 0.07 - 0.1%.

The changes in the apparent density of the samples (Table 5) were similar to those observed for the linear shrinkage values: they grew with the increase in temperature from 1.28 to 2.61 g/cm³.

The minimum values of density after all sintering temperatures

were observed for composition 7, with the maximum amount of slag; composition 2 (100% RM) showed the maximum density value. Such behavior was highly expected, given the ongoing shrinkage of the samples and the reduction of water absorption (porosity) as the temperature increased. Standard deviations are within the limits of 0.09 and 0.4 g/cm³.

Linear shrinkage of the developed ceramics

Changes in linear shrinkage values (Table 5) were analyzed by measuring the largest linear dimensions – samples’ length - after sintering at different temperatures (Figure4).

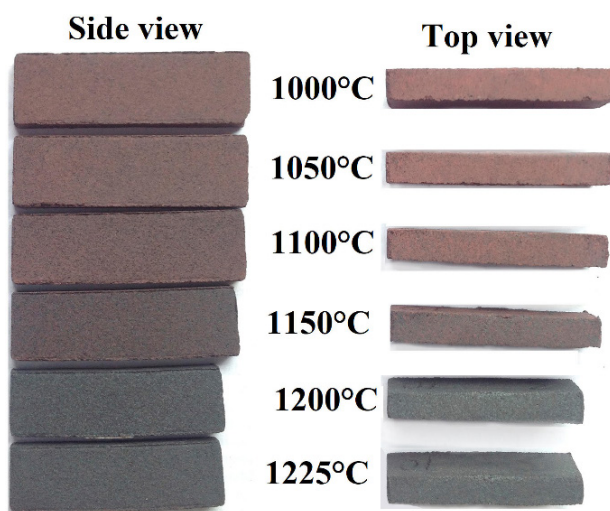


Figure 4: Photo of ceramics 7 after sintering at 1225°C.

In many cases, sharp changes were strongly linked to more significant changes in flexural strength. When the melting point of a sample was exceeded, the shrinkage decreased due

to the foaming of excessive melting through the changes in the color of the samples and the rounding of their edges and angles.

Table 5: Linear shrinkage (%) of ceramics at T °C

Nº	Composites, wt.%			Linear shrinkage (%) of ceramics at T °C							
	NC	RM	BFS	800	900	1,000	1,050	1,100	1,150	1,200	1,225
1	100	0	0	5.36	5.68	7.76	9.09	10.47	11.52	11.95	11.86
2	0	100	0	1.89	2.27	3.42	4.33	5.29	7.24	11.67	12.45
3	0	90	10	0.96	1.08	1.92	2.98	4.30	5.64	9.43	9.56
4	0	80	20	0.54	0.63	0.81	1.51	2.64	4.41	7.40	11.07
5	0	70	30	0.07	0.24	0.31	0.83	2.46	4.38	11.37	12.54
6	0	60	40	0.04	0.11	0.18	0.39	1.69	5.26	12.32	12.35
7	0	50	50	0.08	0.12	0.17	0.44	1.13	4.28	10.99	11.40

The linear shrinkage values increased up to a temperature of maximum strength (Table 3). Shrinkage values were between 0.04 and 12.54%, while their standard deviations ranged from 0.4 and 1.7%.

Physical-chemical processes of structure formation

Composition 7 was chosen to study the physical-chemical processes of the ceramics structure formation due to its high content of RM (50%) and its high flexural strength, exceeding class C demands (>4.0 MPa) of [28].

Mineral composition changes during ceramics sintering

The XRD analyses of the ceramic composition sintered at 1000° and 1225°C (Figure 1-c and d) revealed the presence of magnetite (Fe₃O₄), hematite (Fe₂O₃), fayalite (Fe₂SiO₄), albite (NaAlSi₃O₈), and quartz SiO₂, with a high incidence of amorphous materials. Most of the peaks overlapped to one another. The non-overlapping mineral peaks indicated the noticed reduction or increase in the number of minerals formed between 1000° and 1225°C. It was noticed a significant decrease in the free peaks of fayalite at 2θ° = 34.2° and the almost complete hematite disappearance at 2θ° = 24.2°. It is known that hematite turns into magnetite at high sintering temperatures.

Table 6: Changes in position (d, Å) and intensities (I, %) of XRD peaks of Figure 1-c and -d, ceramic 7 after sintering at 1000 and 1225°C.

2θ°	Comp. 7 -1000°C			Comp. 7 -1225°C		
	d, Å	I, %	Symbol	d, Å	I, %	Symbol
23.9	3.7	53.74	H; A	3.7	28.46	H; A
24.2	3.67	36.73	H	3.6	8.37	H
26.6	3.3	11.57	Q			
33.2	2.69	100.0	H; A	2.69	100.00	H; A
34.2	2.62	15.53	F	2.62	5.17	F
35.7	2.51	68.89	M; H; F; A	2.51	56.76	M; H; F; A
40.9	2.20	21.34	F; A	2.20	17.64	F; A
42.2	2.14	3.84	A	2.16	8.86	A
49.6	1.837	28.13	H; F; A	1.838	23.33	H; F; A
54.2	1.692	33.51	H; F; A	1.691	28.12	H; F; A
57.6	1.598	6.61	H; F; A; Q	1.599	4.26	H; F; A
62.5	1.485	19.98	M; H; F; A	1.484	15.97	M; H; F; A
64.1	1.452	18.89	H; F; A; Q	1.452	13.68	H; F; A

This transformation was not visible in Figure 1 (c and d) due to the absence of free magnetite peaks and their coincidence with hematite, fayalite, quartz peaks, which suffered a decrease or even disappeared in Figure 5-d. Quartz ($2\theta=26.6^\circ$) was the only mineral whose peak did not coincide with and other minerals, disappearing after sintering at 1225°C (Table 6). Albite was the only mineral, which undoubtedly had its intensity increased ($2\theta=42.2^\circ$). A reduction in the intensity scale from 1500 to near 1400 counts per second also indicated that some crystalline phases have turned into the amorphous state. Similar effect of the initial crystalline raw materials during firing was observed by [29]

Thermic reactions during ceramics 7 sintering

The presence of 10.0% SO₃ and high iron content (62.1%, Table 1) in the chemical composition of the blast furnace slag inevitably led to their combination during composition 7's heating in the forms of iron hydrates, iron sulfates, and iron sulfides.

The third exothermic effect of composition 7 (Figure 2-c) occurred at 735° - 1227°C and involved four different thermochemical reactions: the transition $\gamma\text{-Al}_2\text{O}_3 \rightarrow \alpha\text{-Al}_2\text{O}_3$; the transition $\text{Fe}_3\text{O}_4 \rightarrow \text{Fe}$ up to 700-750 °C [25]; reduction in sample weight as a result of the final SO₂ release and burning of the released gas; the formation of Fe₃O₄. The total weight loss of these processes was 4.43%. Probably, the formation of iron dross and the SO₂ combustion process imparted the darkening of the samples, which appeared at temperatures of 1200°C - 1225°C [26, 27]. The maximum intensity of these processes at 1225°C resulted in maximum flexural strength of the ceramics 7.

Morphological structure modifications during ceramics sintering

SEM micro-images from composition 7 after sintering at 1000°C and 1225°C were analyzed, and it was clear the beginning of the initial mix melting process after 1000°C (Figure3-c), with many pores of different sizes between rounded different-sized particles. The escalation in the heating temperature (up to 1225°C) (Figure3-d) led to a complete transformation of the earlier separated particles into a nearly pore-free glass-like monolithic structure. The only explanation for the morphological changes might be variations in the melting of all particles and the chemical interaction that took place.

Flexural strength enhanced almost 2.5 times (19.78 versus 8.12 MPa, Table 3) with significant improvement in other mechanical characteristics. The samples' edges of ceramics 7 were slightly melted, and the surface turned black (Figure 4), apparently due to hematite-to-magnetite transition, which validated the XRD analysis' results.

Microchemical composition of the ceramics' new formations.

The new formations were evaluated by the EDS method (Figure 3-d). Six different point was analyzed, and all of them showed high heterogeneity (Table 7), such as Na content ranging from 0.00 to 7.16%, and Ca content from 0.00 to 7.00%. High heterogeneity, such as Na content ranging from 0.00 to 7.16% and Ca content from 0.00 to 7.00%, was identified in three distinct areas by the EDS method (Table 7 and Figure 3-d). The use of LAMMA (Figure 5) technique has provided similar results in isotopic compositions on the nearest points of the quoted ceramic.

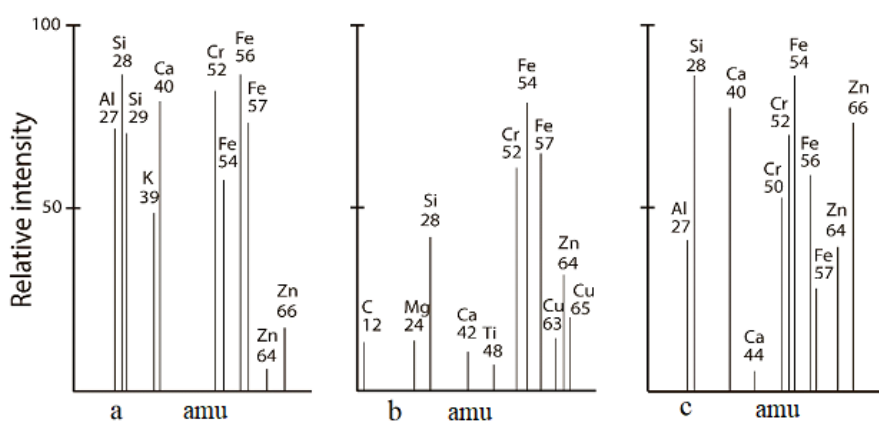


Figure 5: Isotope' laser micro-mass analysis (LAMMA) of the composition 7 new formations sintered at 1,225°C.

Table 7: The chemical composition of the points (Figure 3d) by EDS method.

Points	Na	Al	Si	Ca	Fe	Zr	Total
1	0.00	0.00	19.60	0.00	10.79	69.62	100.00
2	7.16	9.04	13.23	5.48	65.09	0.00	100.00
3	1.96	2.26	4.91	0.00	4.67	86.20	100.00
4	0.00	6.75	11.48	7.00	74.78	0.00	100.00
5	0.00	0.00	0.00	0.00	59.35	40.65	100.00
6	0.00	2.76	23.56	0.00	16.61	57.07	100.00

Environmental characteristics

Gas emission during ceramics sintering

Samples of the heat gases (Table 8) were collected during ceramics’ sintering at 1,225 °C in the glass filter with a thickness

of 0.45µm. The separation of the solid particles deposited on the filter was performed by ultrasound (for three hours in an acidic medium) and determined by the AAS method. These results, along with leaching and solubility tests (Table 9), convincingly confirmed the robust bond of heavy metals in insoluble and non-volatile condition.

Table 8: Gas emission values during ceramics sintering at 1,225°C (by AAS method).

Heavy metals	Compositions, mg/Nm ³	[19]
Cu	1.237	5.0
Cd	0.065	0.2
Pb	0.273	5.0
Cr	0.794	5.0
Ni	0.41	1.0
Zn	1.697	5.0

Table 9: Leaching and solubility of ceramic 7 sintered at 1225°C (by AAS method).

Elements	Leaching, mg/L			Solubility, mg/L		
	Red mud	Comp. 7	[19]	Rd mud	Comp. 7	[19]
As	7.63	0.21	1.0	9.56	< 0.001	0.01
Ba	94.28	< 0.1	70.0	95.47	<0.1	0.7
Cd	7.34	< 0.005	0.5	15.41	<0.005	0.005
Pb	4.43	< 0.01	1.0	7.66	<0.01	0.01
Cr	18.46	< 0.05	5.0	22.67	< 0.05	0.05
Hg	1.47	< 0.001	0.1	3.8	< 0.0002	0.001
Se	2.75	-	1.0	3.35	-	0.01
Al	28.76	< 0.10	*	36.44	< 0.10	0.2
Cu	16.29	< 0.05	*	30.08	< 0.05	2.0
Fe	98.31	0.07	*	108.75	< 0.05	0.3
Mn	55.11	-	*	69.43	-	0.1
Zn	68.48	< 0.10	*	84.13	< 0.10	5.0

Heavy metals solubility and leaching (Table 9) of RM (Zn, Ba, Sn, and Cr) far exceeded the toxicity accepted by the Brazilian standard [19]. But very low melting points of these heavy metals (Zn – 419°C, Sn – 232°, Ba – 727°C) and other chemical elements (K – 63°, Na - 97°, Al – 660°, Ca – 842°C) explains not only the intensification of all developed ceramics' structure formation processes, but also their high chemical stability in acid solutions with remediation of all polluted initial components [30,31].

Therefore, composition 7 was studied for understanding this phenomenon using the AAS method (Table 9). Comparing these values before and after using RM on ceramics production revealed a stable chemical fixation of these metals in RM, culminating in more environment-friendly materials when compared with the requirements of the standard. According to leaching and solubility tests, the developed material presented no propensity to react with the environment. In this way, ceramics might be shredded and recycled as inert material in concrete production at the end of their useful life.

CONCLUSIONS

It has been experimentally demonstrated that bauxite tailings might be used as the main component (up to a content of 80 wt.%) in composites with blast furnace slag. This study aimed to replace the traditional raw materials (natural clay and sand) used to produce environment-friendly red ceramics with suitable mechanical properties. The fifty/fifty red mud and blast furnace slag composition showed 20 MPa in flexural tests, far exceeding the resistance of ceramics made from natural raw materials due to intensification of all structure formation processes. Other useful parameters were observed, such as linear shrinkage values (11.40%), water absorption (1.95%), and moderate density (2.61g/cm³). Physicochemical studies by XRD, SEM with EDC, and LAMMA microanalysis showed that the new ceramics had mainly vitreous structures with small crystal inclusions. The heavy metals leached from RM far exceeded the recommended levels of Brazilian sanitary standards. In the developed ceramics, all heavy metals were tightly bound in insoluble vitreous structures. Furthermore, solubility tests on the new ceramics showed their complete environmental compatibility. Therefore, the application of the suggested method on an industrial scale would have a positive impact on the ecosystems of industrial regions and cities; firstly, preventing the disposal of hazardous waste; secondly, extending the service life of industrial landfills. Finally, decreasing the irreparable impact of quarries of traditional raw materials (clay and sand) for traditional ceramics production.

At the end of the life span of the new ceramics, they might be shredded and used as a filler in concrete production, because they remain utterly inert, demonstrated by the leaching and solubility tests.

The developed materials might be highly profitable because the use of ordinary industrial waste products would significantly reduce the production cost compared to the relatively expensive traditional natural materials.

ACKNOWLEDGEMENTS

The authors are thankful to the staff of the Laboratory of Minerals and Rocks (LAMIR) of the Federal University of Paraná (UFPR), Curitiba, Brazil, for their strong technical assistance during this research.

REFERENCES

1. Hawking SW. <http://www.independent.co.uk/news/science/stephen-hawking>.
2. [pollution-stupidity-artificial-intelligence-warfare-biggest-threats-mankind-a7106916.html](http://www.independent.co.uk/news/science/stephen-hawking).
3. World Aluminum. Primary Aluminum Production. <http://www.world-aluminium.org/statistics/#linegraph> (accessed 22 Jan 2018).
4. Hungary (2018) <https://www.google.com.br/search?q=Hungaria+ecological+tragedy+2010&tbm=isch&tbo=u&source=univ&sa=X&ved=0ahUKEw-jg7rTGjI3ZAhUJEJAKHeP8DxIQsAQIKg&biw=1813&bih=830#imgsrc=endIlyzpvAZ4M>:
5. Mariana, <https://www.theguardian.com/sustainable-business/2015/nov/25/brazils-mining-tragedy-dam-preventable-disaster-samarco-vale-bhp-billiton>
6. Sushil S, Batra VS. (2008). Catalytic applications of red mud, an aluminum industry waste: A review. *J Appl Catalysis B Envir.* 81:1.
7. Liu W, Yang J, Xiao B. (2009). Review on treatment and utilization of bauxite residues in China. *Int J Miner Proc* 3:220-231.
8. Deihimi N, Irannajad M, Rezai B. (2018). Characterization studies of red mud modification processes as adsorbent for enhancing ferricyanide removal. *J Env Man.* 206:266-275.

9. Barthod J, Rumpel C, Calabi-Floody M, Mora ML, Bolan NS, Dignac MF. (2018). Adding worms during composting of organic waste with red mud and fly ash reduces CO₂ emissions and increases plant available nutrient contents. *J Envir Man.* 222:207-215.
10. Dodoo-Arhin D, Konadu DS, Annan E, Buabeng FP, Yaya A, Agyei-Tuffour B. (2013). Fabrication and characterization of Ghanaian bauxite red mud-clay composite bricks for construction applications. *Am J Mat Sci* 3:110-119.
11. Liu Y, Naidu R. (2014). Hidden values in bauxite residue (red mud): recovery of metals. *J Was Man* 34:2662-2673.
12. Pontikes Y, Angelopoulos GN. (2013). Bauxite residue in cement and cementitious applications: current status and a possible way forward. *J Res Con Rec* 73:53-63.
13. Qaidi S, Tayeh BA, Isleem HF, de Azevedo ARG, Ahmed HU, Emad W. (2022). Sustainable utilization of red mud waste (bauxite residue) and slag for the production of geopolymer composites, *J Case St Con Mats* 16:2214-5095):e00994.
14. de Azevedo ARG, Marvila MT, de Oliveira MAB, Umbuzeiro CEM, Huaman NRC, Monteiro SN. (2022) Perspectives for the application of bauxite wastes in the development of alternative building materials. *J Mat Res Tech* 20:3114-3125.
15. ISSUU (2017) Iron and steel slags: global perspective on the circular economy.
16. Lukowski P, Salih A (2015) Durability of mortars containing ground granulated blast-furnace slag in acid and sulphate environment. *J Pro Eng* 108:47-54.
17. Barreto LSS. (2020). Reuse of ornamental rock-solid waste for stabilization and solidification of galvanic solid waste: Optimization for sustainable waste management strategy. *J. Clean. Prod.* 275:122996.
18. El-Ashtoukhy E-SZ, Amin AK, Fouad Y, Hamad HA. (2020). Intensification of a new electrocoagulation system E.-S. Z. characterized by minimum energy consumption and maximum removal efficiency of heavy metals from simulated wastewater. *J Chem En. Proc – Proc. Inten.*154:108026.
19. Kołodyńska D, Hubicki DFZ. (2020) Evaluation of possible use of the macroporous ion exchanger in the adsorption process of rare earth elements and heavy metal ions from spent batteries solutions. *J Chem Eng Proc & Proc Intens.* 147:107767.
20. Jordán MM, López JMR, Almendro-Candel MB, Navarro-Pedreño J. (2022). Technological and environmental behaviour of traditional ceramic bodies obtained by recycling of two types of residues. *J Coatings.* 12:221.
21. Jordán MM, Montero MA, Pardo-Fabregat F. (2021). Technological behaviour and leaching tests in ceramic tile bodies obtained by recycling of copper slag and MSW fly ash wastes. *J Mat Cyc Waste Man.* 23.
22. Mymrin V, Ponte HAM, Ponte JJS, Maul AM. (2005). Structure formation of slag-soil construction materials. *J Mat Str.* 38:107-113.
23. Ding L, Ning W, Wang Q, Shi D, Luo L. (2015). Preparation and characterization of glass--ceramic foams from blast furnace slag and waste glass. *J Mat Let* 14:327-329.
24. Ma.Rincón J. (2018). Vitrification and derived glass-ceramics from mining wastes containing vermiculite and lithium aluminium phosphate. *J Mat Let.* 227:86-89.
25. NBR 10,004. (2004). Solid Waste Classification, Rio de Janeiro.
26. Johnson DW, Gallagher PK. (1971). Kinetics of the Decomposition of Freeze-Dried Aluminum Sulfate and Ammonium Aluminum Sulfate. *J Amer Ceram Soc.* 54:461-465.
27. Kato E, Daemon K, Nanbu M. (1981) Decomposition of two aluminum sulfates and characterization of the resultant aluminas. *J Amer Cer Soc.* 64:436-443.
28. Kimjashov AA. (2010). Phase equilibria in systems Fe - Al - O and Fe - Si - O in the temperature range 1100 - 1300 K, Dissertation, South Ural State University, Chelyabinsk.
29. NBR 15270. (2005). Ceramic components, Part 2: Ceramic blocks for structural masonry and sealing - Terminology and requirements, Rio de Janeiro.

30. Brown ME, Gallagher PK. (2011). Handbook of thermal analysis and calorimetry: recent advances, techniques and applications. Elsevier.
31. Balesteros S, Rincón JMa, Rincón-Mora B, Jordán MM. (2017) Vitrification of urban soil contamination by hexavalent chromium. J Gexplo. 174:132-139.
32. Rincón-Mora B, Jordan MM, Rincón JMa. (2016) Chromium oxide additions in lithium disilicate glass crystallization. J Materials Letters. 179:138-141.